Design of photomagnetic ultra-thin films by electrodeposition of switchable cyanide-bridged Fe 4 Co 4 complexes

Amina Benchohra, Jessem Landoulsi, Niéli Daffé, Christophe Méthivier, Emmanuel Maisonhaute, Laure Fillaud, Jan Dreiser, Michal Studniarek, Marie-anne Arrio, Yanling Li, et al.

Design of photomagnetic ultra-thin films by electrodeposition of switchable cyanide-bridged Fe_4Co_4 complexes.

Amina Benchohra, Jessem Landoulsi, Niéli Daffé, Christophe Méthivier, Emmanuel Maisonhaute, Laure Fillaud, Jan Dreiser, Michal Studniarek, Marie-Anne Arrio, Yanling Li, Sofia Frida Russi, David Kreher,* and Rodrigue Lescouëzec**

This paper is dedicated to the memory of Professor Miguel Julve; the scientist, colleague and friend.

Dr. A. Benchohra, Msc S. Frida Russi, Dr. Y. Li, Prof E. Maisonhaute Prof D. Kreher, Prof. R. Lescouëzec,
Institut Parisien de Chimie Moléculaire, CNRS UMR 8232, Sorbonne Université, 4 place Jussieu, 75005 Paris, France. Rodrigue.lescouezec@sorbonne-universite.fr

Dr A. Benchohra
Laboratoire Chimie, Electrochimie Moléculaires et Chimie Analytique, UMR-CNRS 6521, 6 avenue Victor Le Gorgeu, 29238 Brest Cedex 3, France. Amina.benchohra@univ-brest.fr

Prof D. Kreher
Institut Lavoisier de Versailles, UMR CNRS 8180, UVSQ, Université Paris-Saclay, 78035 Versailles, France. David.kreher@uvsq.fr

Dr. J. Landoulsi, Dr. C. Méthivier
Laboratoire de Réactivité de Surface, UMR CNRS 7197, Sorbonne Université,
4 place Jussieu Paris, 75005, France.

Dr. L. Fillaud,
Laboratoire Interface et Systèmes Electrochimiques, CNRS UMR 8235, Sorbonne Université,
4 place Jussieu, F-75252 Paris cedex 5, France

Dr. Marie-Anne Arrio,
CNRS, Sorbonne Université/IRD/MNHN, UMR 7590, Institut de Minéralogie, de Physique des Matériaux et de Cosmochimie, IMPMC, F-75252 Paris, France

Dr. N. Daffé, Dr. M. Studniarek, Dr. J. Dreiser
Paul Scherrer Institut, CH-5232 Villigen PSI, Switzerland

Keywords: ultra-thin films, molecular switch, photomagnetism, electro-polymerization, surface functionalization, multifunctional materials

Abstract

Preparing thin-films of molecular polymetallic materials remains one of the current limitations in the implementation of polymetallic complexes into devices. The hurdle was tackled here using an electrochemical route for depositing the cyanido-bridged polymetallic complex $\{Tl\subset[Fe^{II}(2\text{-}TPhTp)(CN)_3]_4[Co^{III}(Tp)]_3[Co^{II}(Tp)]\}$(**1**) (where 2-TPhTp = [4-(2-thienyl)Phenyl]tris(pyrazol-1-yl)borate ; and Tp = hydrotris(pyrazol-1-yl)borate), functionalized with thiophene groups, on conductive surface (Pt/mica). Cyclic voltammograms show that the electrochemical pattern of the cubic units is maintained in the electropolymerized film, notably with four quasi reversible successive Fe^{III}/Fe^{II} redox events. Assessing the morphology and the chemical composition of the resulting thin-film by Atomic Force Microscopy (AFM) and X-ray Photoelectron Spectroscopy (XPS) experiments respectively, reveal a homogenous deposition (thickness of *ca*. 20 nm) showing the expected metallic ratio. More importantly, X-ray Absorption Spectroscopy (XAS) and X-ray Magnetic Circular Dichroism (XMCD) measurements demonstrate that the photo-induced metal-metal electron transfer is preserved in the film. XMCD signals of Fe and Co atoms at their $L_{2,3}$ absorption edges both indicate an equivalent conversion of Fe^{II}-CN-Co^{III} diamagnetic pairs into Fe^{III}-CN-Co^{II} paramagnetic ones under laser light irradiation below 62 ± 5 K. As for the photomagnetic complex, the phenomenon is reversible: the metastable Fe^{III}-CN-Co^{II} paramagnetic pairs thermally relax to the diamagnetic ground state upon heating to room temperature.

Introduction.

Molecular magnetic switches (MMS) are complexes, the electronic configurations of which can be reversibly modified under the application of an external stimulus, *e.g.* light, temperature or pressure change, magnetic or electrical fields.[1–3] The resulting spin-state change can lead to a modification of the magnetic properties but also of the optical, dielectric or mechanical ones. Accordingly, the molecular magnetic switches have been the subject of active research, whether it is for an in-depth understanding of the switchable phenomena or to harness their utility as molecular sensors, actuators or memories in technological applications.[4–12] To date, the most investigated molecular magnetic switches are spin-crossover complexes (SCO), particularly those based on Fe(II) octahedral entity, which can show drastic physical changes upon converting from the Low-Spin $(t_{2g})^6$ configuration (S = 0) to the High-Spin $(t_{2g})^4(e_g^*)^2$ paramagnetic one (S =2). Important research efforts were devoted to deposition methods of SCO molecular switches on surfaces to create original electronically-active interfaces[13–16], with promises in the fields of molecular electronics and spintronics.[4–6][20] Another interesting class of magnetic switches gathers polymetallic materials displaying metal-to-metal electron transfer coupled to a spin transition. The first report on photoswitchable charge-transfer (CT) complexes dates back to 1996,[21] on FeCo Prussian Blue Analogues (PBAs), a class of insoluble cyanido-based inorganic polymers of which diamagnetic Fe^{II}_{LS}-CN-Co^{III}_{LS} and paramagnetic Fe^{III}_{LS}-CN-Co^{II}_{HS} pairs can be reversibly converted from one to another. A large number of discrete polymetallic systems mimicking the switchable properties of the PBA polymers were developed over the last decades.[22,23] However, in contrast to SCO monometallic complexes, the integration of switchable polymetallic charge transfer molecules (as thin films, nano-objects and composite materials) into devices remains almost unexplored, although interesting coupling between the electronic-state switching and applied electric field can be expected.[24–26]

An interesting seminal work was published by Clérac and coworkers[27] on a rare example of Micro-Electro-Mechanical (MEM) sensor including a photo and thermo-switchable charge transfer octametallic complex. The device was obtained by drop casting a micrometric layer of the molecular switch on a piezoelectric resonator, resonance frequency variations of which correlated with the volume change accompanying the high-spin─low-spin conversion of the molecules.

One of the current challenges of designing molecule-based devices often remains the first step, consisting in the deposition of the functional molecules on surfaces (by chemi- or physisorption) as sub-monolayer (or isolated molecules)[8] or as low-dimensional thin-films.[28,29] Aside from restricted examples, the switchable properties of surface-bound magnetic switches layer (or thin-films) are often altered, if it is not the structural integrity of interfacial MMS that is lost.[9,30,31] Currently, thermal (vacuum) sublimation remains the prevailing technique for preparing high-quality and contamination-free films of molecular switches since its first demonstration on the Fe(II) mononuclear spin crossover (SCO), $[Fe(phen)_2(NCS)_2]$.[32] However, owing to the experimental requirements that the molecular candidates should meet to prepare films by evaporation (*i.e.* thermally stable at sublimation temperature, neutral, a crystalline lattice free of solvent), thermal sublimation precludes a significant number of magnetic switches, notably discrete polynuclear entities. For this reason, the deposition of polymetallic molecular switches was explored in solution with techniques such as Langmuir-Blodgett method[33] or static-spray deposition,[34] yet the number of reports is very limited. Beyond general hurdles associated with surface deposition (*i.e.* molecule degradation, hybridization and properties loss), the polymetallic molecules properties must naturally meet the deposition technique requirements. In solution, it implies for instance favorable physico-chemical features such as a good solubility in selected organic solvents and a high thermodynamic stability.

In that context, our group dedicated efforts over the past decade to investigating the properties of a family of cyanide-bridged octametallic complexes, A $\subset\{Fe_4Co_4\}$ (where A is a monovalent cation = Cs^+, Rb^+, Tl^+, K^+, and where the metal ions are coordinated with tris(pyrazol-1yl)borate), which proved be remarkably stable in solution in various organic solvents.[35,36] Beyond its role as a negative charge balance and as a template in the polymetallic edifice, the inserted cation confers a stability, which increases with increasing the cation size through interactions with the cyanide bridges. Interestingly, the $A\subset\{Fe_4Co_4\}$ molecular core properties retain a dependency on the inserted cation, just as the 3D Fe/Co PBA network.[37] In addition to their photo-switchable magnetic properties, these cages possess impressive redox features, *i.e.* a great stability over a large electrochemical window and up to nine accessible redox states.[36] Finally, the synthetic versatility of the tris(pyrazol-1-yl)borate ligands family offers a various choice of functionalization[38–40] opening different possible routes for the integration of these molecular $A\subset\{Fe_4Co_4\}$ switches into materials. A recent demonstration was thus provided by our group with the adsorption of $A\subset\{Fe_4Co_4\}$ cages, substituted with aryl-thiophene on Co sites, on Au(111) substrates by harnessing the electrospray ionization process.[41] This soft deposition strategy enabled a submonolayer coverage while maintaining the molecular structure of the physisorbed material.

In the present work, we explored the electropolymerization technique, as a soft-chemistry approach, for depositing an analogous $A\subset\{Fe_4Co_4\}$ cage on conductive substrates as ultra-thin films. For this purpose, the $A\subset\{Fe_4Co_4\}$ core was functionalized with peripheral thiophene groups allowing the electrodeposition of the functionalized polymetallic cubic complex.

To the best of our knowledge only one analogous attempt on discrete charge transfer (CT) polymetallic switches was described by Oshio and co-workers in 2011.[42] The authors successfully isolated a cyanide-bridged $\{Fe_2Ni_2\}$ square bearing terthiophene substituents, but

subsequent electropolymerization experiments of the coordination complex led to its decomposition. This could be explained by the association/dissociation equilibria in solution occurring for polymetallic complexes with labile Ni(II) ions.

Herein we report a thorough investigation on the design and characterization of homogeneous ultra-thin films through the electropolymerization of an unprecedented thiophene-functionalized cyanide-bridged Tl⊂{Fe_4Co_4} cages (Figure 1), while maintaining both the switchable redox and photo-magnetic properties of the starting molecular compounds. For this purpose, we prepared the polymetallic building-block {Tl⊂ [Fe^{II}(2-TPhTp)$(CN)_3$]$_4$[Co^{III}(Tp)]$_3$[Co^{II}(Tp)]} **(1)** (where 2-TPhTp = [4-(2-thienyl)Phenyl]tris(pyrazol-1-yl)borate ; and Tp = tris(pyrazol-1-yl)borate). The latter cage properties, of simplified formula {Tl ⊂ [Fe(2-TPhTp)$_4$Co(Tp)$_4$]}or Tl ⊂{Fe_4Co_4}, represent the best compromise between solution stability and the photo-magnetic response. The optimal position of the thiophene, on the Fe vertices rather than on the Co ones, was guided from a former study on the influence of the functionalization on the cage switchable properties.[43] It was observed that the substituent's impact on the photomagnetic properties of the A⊂{Fe_4Co_4} core was optimized when positioned on Fe sites. The present work first describes the multi-step synthesis of this starting molecular material along with the full characterizations of its electronic properties. Their deposition as ultra-thin films on Pt substrates was conducted by cyclic voltammetry experiments and the composition, homogeneity and thickness of the resulting film were assessed by X-ray photoelectron spectroscopy (XPS) and atomic force microscopy (AFM) measurements. Moreover, the switchable photomagnetic properties of the electropolymerized film are examined in-depth through X-ray absorption spectroscopy (XAS) and X-ray magnetic circular dichroism (XMCD) characterizations.

RESULTS AND DISCUSSION

Synthesis and characterizations of the functionalized molecular polymetallic unit, Tl ⊂ {Fe(2-TPhTp)$_4$Co(Tp)$_4$} (1).

Functionalizing the {Fe_4Co_4} molecular core, with thiophene on iron sites, requires a multistep synthesis (Scheme S1), including the preparation of a thiophene-functionalized tricyanido heteroleptic Fe(III) complex (**C**). For this purpose, the [4-(2-thienyl)phenyl)trimethylsilane] was converted into its tris(pyrazolyl)borate equivalent, 2-TPhTp (**A**, Scheme S1), adjusting reported synthetic routes for the preparation of third-generation scorpionates derivatives (see detailed procedures and characterizations in SI).[41,44,45] Stoichiometric reaction of 2-TPhTp (**A**) with the ferrous salt $Fe(BF_4)_2.6H_2O$ afforded the corresponding homoleptic Fe(II) complex (**B**) which subsequent cyanidation led to the anionic $[Fe^{II}(2\text{-}TPhTp)(CN)_3]^{2-}$ building block that was finally oxidized into $[Fe^{III}(2\text{-}TPhTp)(CN)_3]^-$ (**C**). The self-assembly reaction of the latter $[Fe^{III}(2\text{-}TPhTp)(CN)_3]^-$ precursor with the Co^{II} salts was conducted, in acetonitrile at room temperature, with an excess of Thallium(I) hexafluoroacetylacetonate, Tl(hfac). The elementary hydrotris(pyrazol-1-yl)borate scorpionate ligand was then added to complete the Co ions coordination sphere, affording thus the target thiophene-functionalized molecular switch {Tl ⊂ [Fe(2-TPhTp)$_4$Co(Tp)$_4$]} (**1**, Figure 1B) in moderate yield (Y: 25%). As observed for similar Fe/Co cubic compounds,[28-29] some electron transfers occur during the synthesis leading to a neutral mixed-valence complex, $\{Tl\subset [Fe^{II}(2\text{-}TPhTp)_4][Co^{III}(Tp)]_3[Co^{II}(Tp)]\}$, consisting of three $\{Fe^{II}\text{-}CN\text{-}Co^{III}\}$ pairs and a $\{Fe^{II}\text{-}CN\text{-}Co^{II}\}$ one, which resulting negative core charge is compensated by the inserted Tl^+ cation.

The molecular structure and composition of (**1**) were first confirmed by High-Resolution Mass Spectrometry (HRMS), FT-IR and NMR spectroscopy. Characteristic mass spectrometry peak of the complex (**1**) was identified at *m*/*z* = 3313.4160 for the $\{Tl\subset[Fe^{II}(2\text{-}TPhTp)_4Co^{III}(Tp)_4]\}^+$ form resulting from an *in-situ* oxidation (Figures S13-S14). The IR

spectrum (Figure 1A, S3) shows typical cyanide stretching vibrations (ν_{CN}) in the 2000-2300 cm^{-1} range. As inferred in related studies,[46] the intense cyanide stretching located at 2106 cm^{-1} and the shoulder at 2121 cm^{-1} are associated to the $\{Fe^{II}\text{-}C\equiv N\text{-}Co^{III}\}$ linkers while a shoulder corresponding to $\{Fe^{II}\text{-}C\equiv N\text{-}Co^{II}\}$ segments appears at 2091 cm^{-1}. Moreover the two B-H stretching vibrations at 2523 and ca. 2490 cm^{-1} point to the occurence of two distinct redox states for the Co ions linked to the Tp ligand, the higher one being assigned tot the Co^{III} state and the lower one to the Co^{II} one. The EPR spectra recorded in frozen DCM and in solid state spectra at 5 K (Figure 1C, S15) are consistent with the presence of a unique paramagnetic Co^{II}_{HS} ion, the other Fe^{II}_{LS} and Co^{III}_{LS} ions being all diamagnetic. The EPR signal is typical for an isolated octahedral Co^{II}_{HS} ion with a S = ½ effective spin and an axial anisotropy. The measured *g* values of $g_{eff\perp}$ = 1.87 and $g_{eff\text{II}}$ = 7.7, compared well with those obtained on related cubic complexes.[36] The electronic state of the cube is also supported by the magnetic susceptibility temperature product ($\chi_M T$) value measured per cubic unit at 300 K, 2.7 $cm^3.mol^{-1}.K$, which corresponds to the expected value for one Co^{II}_{HS} ion. The 1D ^1H NMR spectrum displays a spectral pattern spread over a large paramagnetic window owing notably to protons in the vicinity of the Co^{II}_{HS} ion (Figure S10). A set of 29 signals over the 30 expected was observed for the $Tl\subset\{Fe^{II}_4Co^{III}_3Co^{II}\}$ cube (**1**), which can be roughly described by an average C_3-symmetry similarly to this family of derivatives (see details SI, NMR section). The remaining signal being attributed to a {H-B} proton resonance that is not always detected at this temperature.

The conversion of the electronic states of the functionalized cube following potential variations or photo-irradiation was checked by cyclic voltammetry (CV) and photomagnetic studies. The photomagnetic properties of (**1**) were measured at 20 K in solid state (Figure 1E, S16). Irradiation of the sample with a 808 nm laser source (P = 0.217 W. cm^{-2}) induces a conversion rate of diamagnetic $\{Fe^{II}\text{-}Co^{III}\}$ heterometallic pairs to paramagnetic $\{Fe^{III}\text{-}Co^{II}\}$

ones with a maximum value of $\chi_M T$ (8.75 $cm^3.mol^{-1}.K$) after 10 min (Figure 1E). Subsequently, heating the sample at 0.3 K min^{-1} reveals the relaxation temperature of the metastable state T_{relax} = 60 ±2 K (Figure S16).

As well illustrated in literature with cyanide-bridged complexes,[47] the pairing of transitions metals *via* a short bridge as cyanide can lead to multiple electrochemical response spread over a large electrochemical range. As observed in previous works,[48,49] four Fe^{II}/Fe^{III} chemically reversible redox processes appear successively between 0.9 and 1.5V (vs SCE), as distinct events (Figure 1F, Table S1). Low separation between the peak potentials is observed, as a consequence of a low reorganization energy within the coordination sphere. In contrast, the Co^{II}/Co^{III} redox processes appear at lower potentials [-1; 0.5V] (vs SCE) and are electrochemically irreversible (Figure S17). The large peak-to-peak separation (meaning the difference between the oxidative and reduction potentials) results from an important reorganization of the coordination sphere of the Co ion induced by the high-spin—low-spin conversion accompanying the electron transfer process. Finally, the thiophene-aryl derivate anodic potential (E^{ox}_{thio}) occurs at 1.57 V (*vs* SCE).

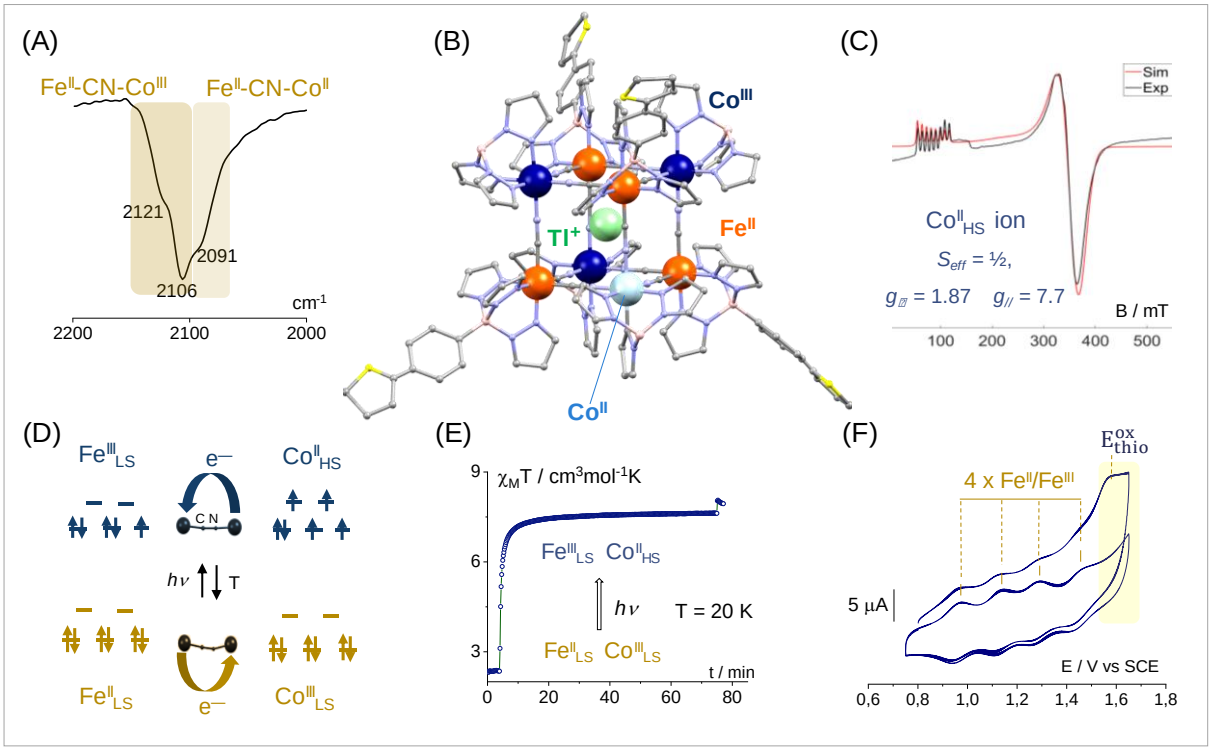

Figure 1. (B) Simulated structure of the Tl ⊂{Fe(2-TPhTp)$_4$Co(Tp)$_4$} cubic switch (**1**), depicted together with its molecular characterizations (A, C, E, F). Fe^{II} ions are shown in orange, Co^{III} in dark blue, Co^{II} in light blue, Tl^{+} in green, S in yellow, N in violet, B in pink and C in grey. Hydrogen atoms are omitted for clarity. (A) FT-IR spectrum of (**1**) centered on the cyanide stretching bands, recorded on its crystalline powder. (C) EPR spectrum of (**1**) in DCM at 4K (D) Scheme of the metal-to-metal electron transfer coupled to spin-transition (ETCST) process responsible for the switchable magnetic properties. (E) Plot of χ_mT versus irradiation time of (**1**) in solid state (20K), under a 808nm light irradiation. (F) Cyclic voltammogram of (**1**), centered on the range of Fe^{II}/Fe^{III} and thiophene redox processes, in ACN (10^{-4}M) with 0.1M TBAPF$_6$ using a glassy carbon as working electrode and a saturated calomel electrode as reference at 0.1V.s^{-1}.

Deposition of the molecular switch (1) on surface as electropolymerized thin-films.

The study of the electrochemical polymerization of (**1**) was conducted using two types of working electrodes, a glassy carbon disk electrode (Figure S17-S19) or a Pt/mica substrate (Figure 2). Standard electrochemical characterizations and demonstration of the adsorption of the electrogenerated material to the electrode surface were carried out with the glassy carbon electrode. By using an easy-to-handle electrode such as a Pt/mica substrate, the scope of investigations was enlarged to microscopic and spectroscopic surface measurements (AFM, XPS, XAS and XMCD).

In both cases, the electrodeposition was performed in a 10^{-4}M acetonitrile solution of (**1**) with 0.1M of Bu_4NPF_6. applying five sweeps over the potential range -1 to 1.85 V (vs SCE). Over the first cycle, the cyclic voltammograms (obtained Figure 2 with the Pt/mica electrode, Figure S17 with the glassy carbon one) display the typical electrochemical pattern of these Fe/Co polymetallic complexes as discussed above (Figure 1F) added to the irreversible oxidative wave of the thiophene-aryl moiety (at 1.57V vs SCE). Successive potential sweep result in the attenuation of thiophene-aryl moiety peak (E^{ox}_{thio}) (Figure 2B, Figure S17) and the appearance, as anticipated, of an oxidation wave at lower anodic potential (0.79V vs SCE) corresponding to the bithiophene derivatives newly formed (depicted Figure 2B). According to the broadly accepted mechanism, the electropolymerization of thiophene species is initiated by the formation of a thiophene radical cation at the monomer oxidation potential (being here E^{ox}_{thio}),[50] as depicted scheme S2. The following step implies the reaction of two oxidized monomer unit affording then a dicationic dimer and the reaction completes with the loss of two protons. Finally, the propagation process produces polymeric species that precipitate at the surface electrode when their solubility limit is reached. With four polymerizable sites per cube, the final polymeric material can reasonably be envisaged as a highly branched 3D-architecture, with cubic units separated by a maximum sequence of two paired{aryl-thiophene} segments. The electropolymerization of these multiple reactive-sites $\{Fe_4Co_4\}$ monomers proceeds without structural control leading to a varying number of polymerized sites per cube, and thus an unpredictable number of 'chain-ends'. Structural inhomogeneities may also be reinforced by additional factors such as a decrease of the accessibility of thiophene sites during the polymer growth.

It is also worth noting that upon cycling the Fe^{II}/Fe^{III} redox processes remain well resolved while the ones involving Co^{II}/Co^{III} ions are less defined. To explain this latter point, hypotheses suggested consider the influence of (i) the slow kinetic of these processes, (ii) the importance of the background charging current of the electrolyte and possibly (iii) the various

chemical environments of the Co ions which could lead to shifts in the standard potentials and electron transfer rate constants.[51]

To ascertain the adsorption of the electrodeposited material on the electrode surface, the coating was washed several times with pure acetonitrile, after which its electroactivity was measured at different scan rates in acetonitrile containing 0.1M of $TBAPF_6$. Consistent with the polymerization process and the related literature[52], the thiophene oxidation wave disappeared as shown Figure S18 in the cyclic voltammograms of the electropolymerized thin-film (on the glassy carbon electrode). The redox signature of the octametallic framework was preserved, as evidenced by the distinctive characteristic Fe^{II}/Fe^{III} redox processes in the range of 0.9 to 1.5 V (vs SCE). For instance in figure S18 a), their bell-shaped curves are observed clearly with a very small peak-to-peak separation ($\Delta E = E^{ox}-E^{red}$) as expected for diffusionless electron transfer of immobilized species. Lastly, analyses of the oxidative peak currents of the iron ions as function of scan rate reveal a linear correlation typical of adsorbed species (Figure S19).

As mentioned above, microscopic and spectroscopic investigations were conducted on samples electropolymerized on Pt/mica substrates (Figure 2). The chemical composition of the consequent electropolymerized film was examined by XPS analysis, which is suitable to probe the surface at a depth of a few nanometers, and to provide information regarding the chemical environment of atoms. Figure 3A presents typical Co 2p, Fe 2p and Tl 4f peaks recorded on the electropolymerized film. The Co 2p doublet shows contributions at about 782.6 and 797.7 eV due to Co $2p_{3/2}$ and Co $2p_{1/2}$ respectively, with a consistent distance between their positions (15.1 eV). A satellite contribution can also be observed through the shoulder around 788.5 eV (Figure 3A). The peak positions and line shape of the observed Co 2p XPS spectrum are similar to the earlier report[41] indicating mixed valence Co(II/III) ions with a dominating presence of Co(III), as expected for the paramagnetic Fe/Co entity. The Fe 2p peak also shows a well-defined Fe $2p_{3/2}$ and Fe $2p_{1/2}$ doublet contributions at about 708.4

and 721.2 eV respectively, which are clearly attributed to Fe(II) species. The Tl 4f peak shows a doublet at about 120.4 and 124.8 eV due to $4f_{7/2}$ and $4f_{5/2}$, respectively, in agreement with values reported for thallium(I) salts.[53] The experimental values of Co/Fe and Tl/Co molar concentration ratio deduced from XPS measurements (of 0.90 and 0.27 respectively) are in agreement with the stoichiometric theoretical values of $\{Tl \subset [Fe(2\text{-}TPhTp)_4Co(Tp)_4]\}$ structure (*i.e.* 1 and 0.25 respectively). The S 2p peak was decomposed into one main doublet with S $2p_{3/2}$ component at 164.3 eV, a distance between S $2p_{3/2}$ and S $2p_{1/2}$ components equal to 1.1 eV, the same FWHM and a ratio of 2 imposed between their respective intensities (Figure S22). The latter signal corresponds to the S atoms in the thiophene ring structure of the 2-TPhTp ligand. The presence of oxidized sulfur species were also detected showing a doublet with S $2p_{3/2}$ component at about 168.6 eV, but the molar concentration of oxidized sulfur does not exceed about 15% of the total sulfur probed by XPS. XPS analysis also revealed the presence of P and F elements at a low amounts, originating from the PF_6^- anions present in the supporting electrolyte, and probably inserted in the film during the electropolymerization process.

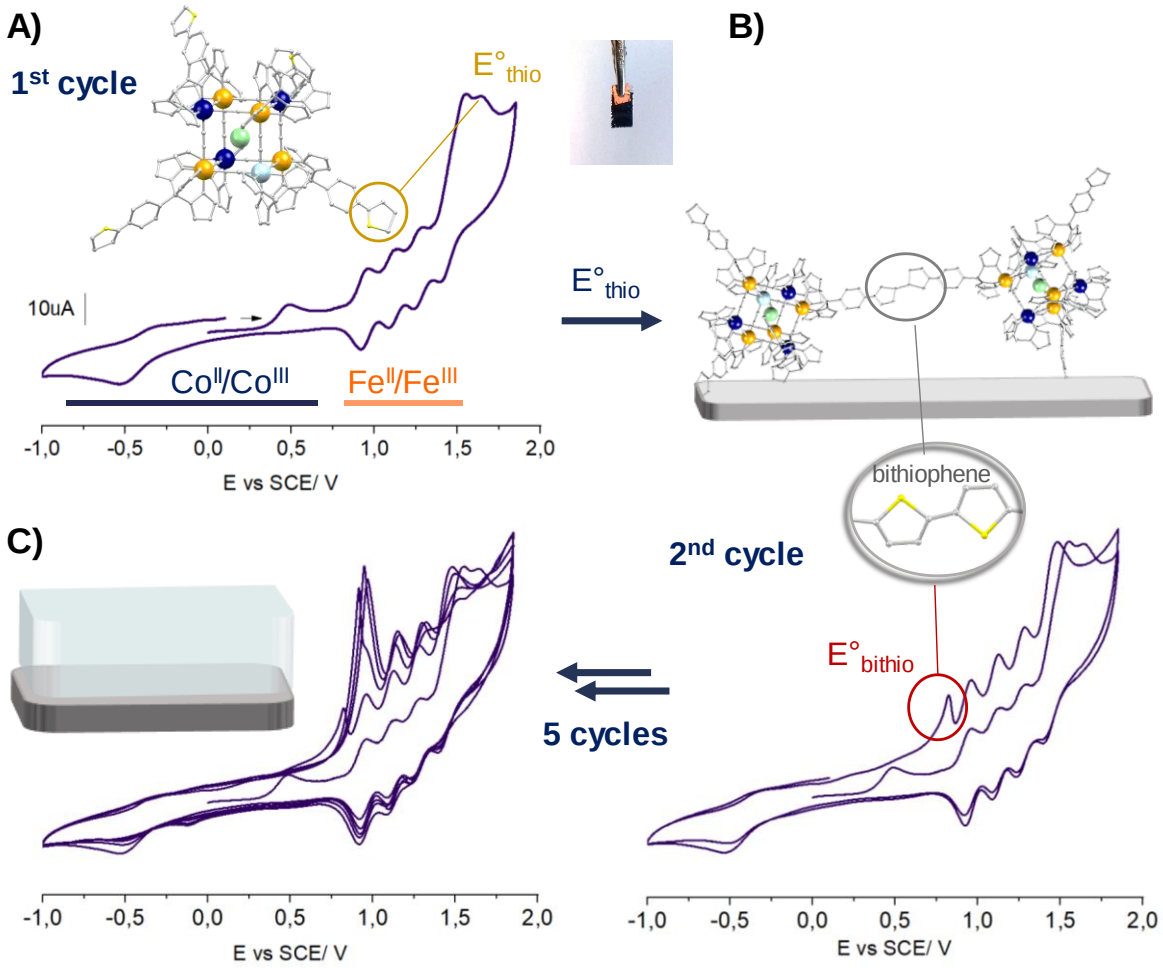

Figure 2. Sequential scheme of the electropolymerization of {Tl ⊂ [Fe(2-TPhTp)$_4$Co(Tp)$_4$]} (**1**) on a Pt surface using consecutive cyclic voltammetry. Cyclic voltammograms in a 10^{-4}M acetonitrile solution of (**1**) with 0.1M $TBAPF_6$, using a Pt/mica substrate as working electrode (picture): A) after the first potential sweep. B) after the second cycle revealing the oxidative wave of the bithiophene groups newly formed. C) after five consecutive potential sweeps. All measurements were carried out at v= 100 mV.s^{-1} Note: In scheme, the cube framework is pictured in grey with the color identification of the following elements: Fe^{II} ions are shown in orange, Co^{III} in dark blue, Co^{II} in light blue, Tl^{+} in green, S in yellow. Hydrogen atoms are omitted for clarity

The morphology of the electropolymerized film on Pt substrate was probed by atomic force microscopy (AFM) in the dried state. A typical height image is given in Figure 3B, revealing a uniform and a relatively smooth surface (R_{rms} = 2.56 nm, computed from 2 µm × 2 µm image). The main topography consists of fairly regular packing of nanoparticles with a mean height which does not exceed about 5 nm, except for a few isolated aggregates (see the scan line in Figure 3B). However, the real particle height could not be evaluated reliably because

the tip was too large to penetrate into the interstices between particles. The thickness of the electropolymerized film was estimated by AFM in the dried state by scratching the film locally and measuring the step height between the film and the scratched area (Figure S20). For this purpose, a surface of 2 µm × 2 µm was scratched by the AFM tip at a high applied force, yielding a rectangular footprint, as shown in Figure 3C. By exploring several scratched areas, the film thickness, determined using line scan crossing the frontier of the scratched area, was shown to have an average thickness of 22.3 ± 1.1 nm. Approximating the cage volume as a hard sphere, a rough estimation of its radii, extracted from the simulation Figure 1B, gives ~1.5nm. In that respect, the coating can be considered as approximatively a seven-layer film.

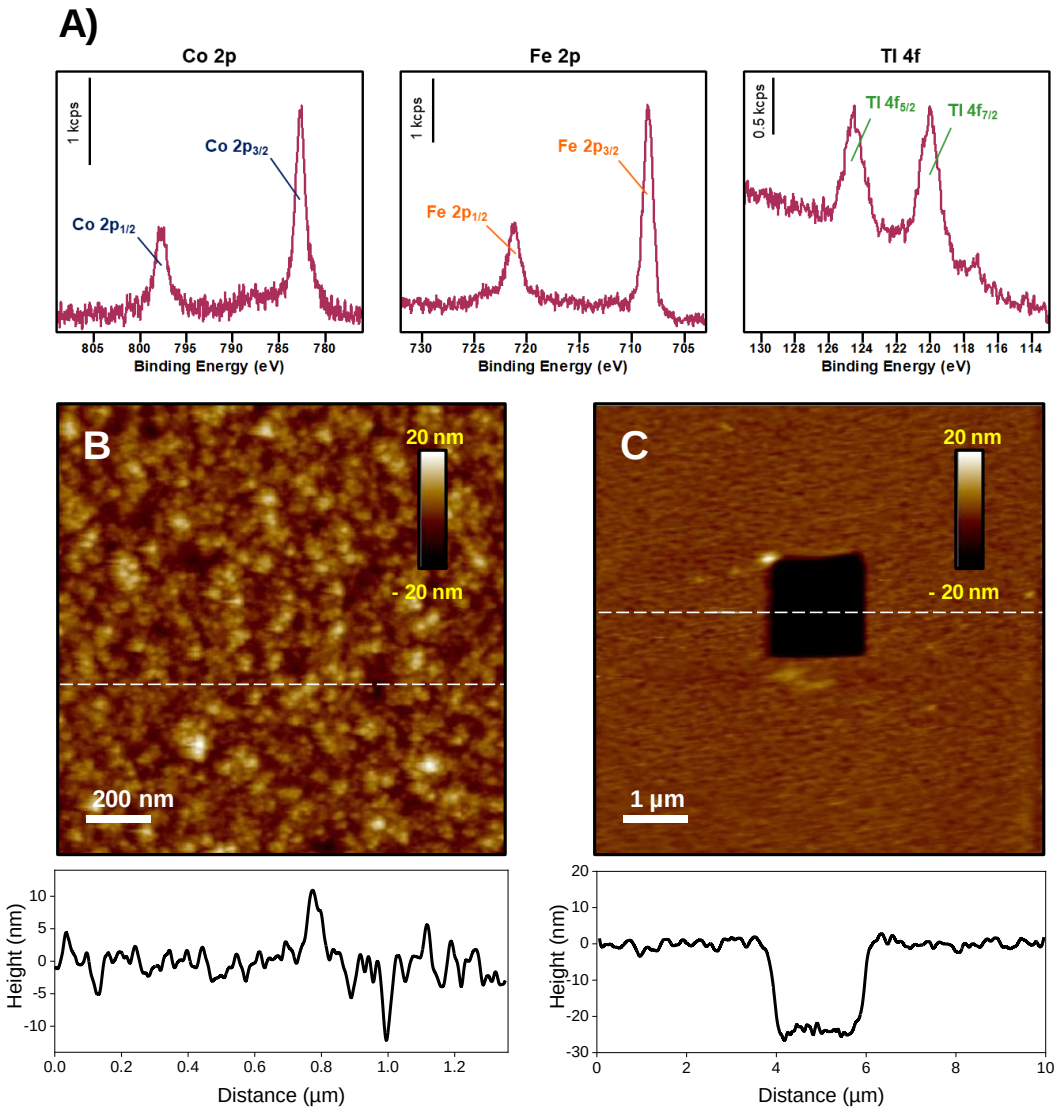

Figure 3. A) Representative Co 2p, Fe 2p and Tl 4f peaks recorded on {Tl ⊂ [Fe(2-

TPhTp)$_4$Co(Tp)$_4$]}electropolymerized thin-films on Pt/mica substrate (illustrated figure 2). Representative AFM height images B) (2 µm x 2µm; Peak Force Tapping, in air) recorded on the {Tl ⊂ [Fe(2-TPhTp)$_4$Co(Tp)$_4$]} electropolymerized thin-film on Pt/mica; C) (10 µm x 10µm ; Contact mode; in air) recorded after scratching part of the film (5V, 3Hz). The dark central square corresponds to the scratched area (from which the film was removed). Line scans were taken at the location indicated by dashed lines. Arrows indicate the vertical distance between the top of the film and the presumable underline substrate.

In order to probe the photo-sensitivity of the electropolymerized thin-film deposited on Pt, XAS and XMCD experiments were carried out using synchrotron radiations (Figure 4, S23-26). XAS spectra were acquired successively at the Fe and Co $L_{2,3}$ edges by collecting the drain current on the samples across incident photon energies ranging from 700 to 740 eV and 770 to 810 eV respectively. **Figure 4** shows the experimental spectra measured on the electropolymerized thin-film in the initial state at 300 K (before irradiation) and the photo-excited state at 2 K after irradiation with a LED source (λ=780 nm, Power =18mW). Interestingly, comparison analyses with our previous study on the {Cs⊂ [Fe^{II}(Tp)(CN)$_3$]$_4$[Co^{III}(pzTp)]$_3$[Co^{II}(pzTp)]} cage, abbreviated {Cs⊂ [Fe(Tp)$_4$Co(pzTp)$_4$]} (with pzTp = tetra(pyrazol-1-yl)borate), deposited on surface by drop-casting,[54] revealed identical spectroscopic fingerprints for the electropolymerized thin-film. Additionally, the electronic XAS signatures of the Co^{III}_{LS}, Co^{II}_{HS}, Fe^{II}_{LS} and Fe^{III}_{LS} metal ions of the archetypal {Cs⊂ [Fe(Tp)$_4$Co(pzTp)$_4$]} cage were ascertained by Fe and Co $L_{2,3}$ edges measurements and multiplet calculations.

In that sense, at 300K meaning in the initial state, the Fe L_3 edge recorded on the electropolymerized thin-film is characterized by a double peak feature corresponding to the electronic signature of Fe^{II}_{LS} ions. On their side, the Co $L_{2,3}$-edges XAS signal present a mix of the electronic signature of Co^{III}_{LS} (dominant feature at 779.26 eV) and Co^{II}_{HS} (lower energy peaks at 775.1, 776.7 and 777.9 eV). The spectra obtained on the initial and photo-excited states of the electropolymerized thin-film can be reproduced by a linear combination of Co^{III}_{LS}, Co^{II}_{HS}, Fe^{II}_{LS} and Fe^{III}_{LS} single XAS spectra (Figure S23) measured on the following compounds

used as references: (i) a diamagnetic cage Cs $\subset$\{[Fe^{II}(Tp)$(CN)_3$]$_4$[Co^{III}(2-TPhTp)]$_4$\}ClO_4 for low-spin Co(III) ions, (ii) the homoleptic complex [Co^{II}(2-TPhTp)$_2$] for high-spin Co(II) ion, and the cyanide building-blocks (iii) K_2[Fe^{II}(Tp)$(CN)_3$] and (iv) NBu_4[Fe^{III}(Tp)$(CN)_3$] for the low-spin Fe(II) and Fe(III) ions respectively.

Quantitative treatments give for the electropolymerized thin-film at 300K, *i.e*. in the ground state, 100 % of Fe^{II}_{LS} and a mix of 90±2 % of Co^{III}_{LS} (10±2% of Co^{II}_{HS}). These values indicate a higher Co^{III} content compared to that found in the pristine compound (**1**) for which best fits of the initial state (*i.e.* at 300 K) are obtained using 100% Fe^{II}_{LS} at the Fe *L*-edges, 75% of Co^{III}_{HS} (25% of Co^{II}_{HS}) at the Co *L*-edges (Figure S24). XMCD spectra of the electropolymerized thin-film (Figure S25) were also recorded before light irradiation at 200 K, well above the relaxation temperature of (**1**) deduced from photo-irradiation studies mentioned above. Furthermore, at 200 K, no XMCD signal was detected both at the Fe and Co $L_{2,3}$ edges which is consistent with a ground state solely consisting of Fe^{II}_{LS} diamagnetic metals ions. Regarding the cobalt ions, the absence of an associated dichroic signal confirms a negligible contribution of Co^{II}_{HS}, probably below the detection limit at our experimental conditions. The different ratio of cobalt ions valence states observed between the pristine compound (**1**) and the electropolymerized film, is tentatively explained by a sensitivity of the thin-films toward oxidation overtime.

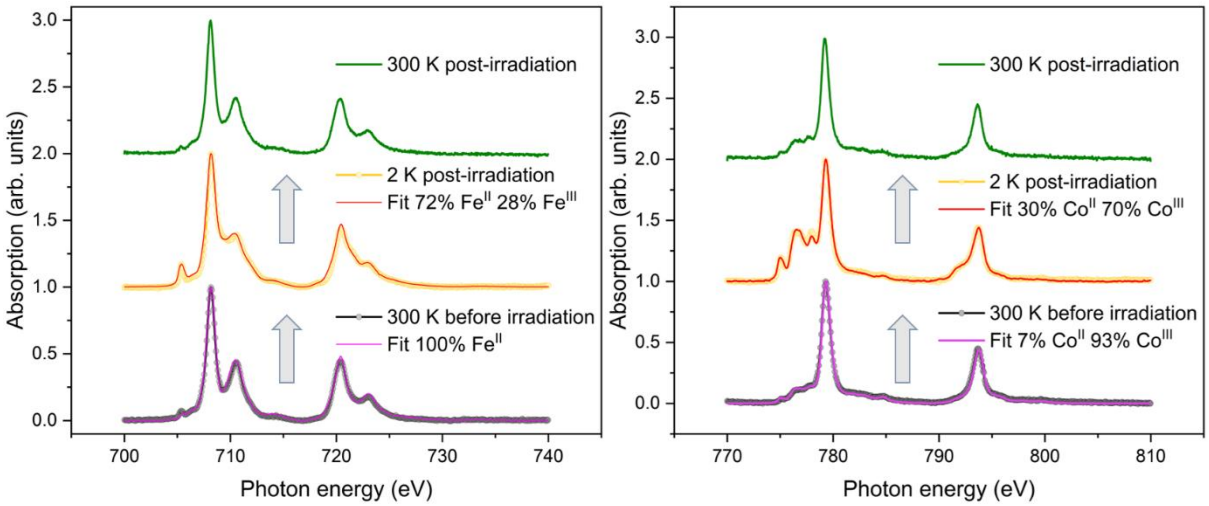

Figure 4. Fe (left panel) and Co (right panel) $L_{2,3}$ edges XAS spectra measured on the electropolymerized film of (**1**) before LED irradiation at T= 300 K (violet), after light-irradiation at 2 K (yellow) and after light conversion at 300 K (green). Best fits of the initial and excited states are obtained by linear combination of XAS measured on reference sample for Co^{III}_{LS}, Co^{II}_{HS}, Fe^{II}_{LS} and Fe^{III}_{LS}.

After irradiation of the electropolymerized thin film at 2 K, the modifications of the XAS spectral features at both Fe and Co *L*-edges evidence the occurrence of a light-induced process converting the Fe^{II}_{LS} ions into Fe^{III}_{LS} with the reduction of the peak at 710.6 eV and the appearance of a peak at 705.4 eV, the latter matching the electronic signature of Fe^{III}-CN linkers. Simultaneously, an increase of the Co^{II}_{HS} ions is also observed with more intense features with respect to the electronic signature of Co^{III}_{LS} ions. This result is in line with the XMCD signals reported in Figure S25. Indeed, both Fe and Co XMCD signal were detected after irradiation of the thin film at 2 K, demonstrating the presence of the paramagnetic metal ions in the light-induced excited state of the electropolymerized molecular cages.

The composition of the excited-states in the thin-film was extracted from linear combination of the single metal ions references (mentioned above) leading to 72±1 % Fe^{II}_{LS} + 28±1 % Fe^{III}_{LS} on the one hand and 40±1 % of Co^{II}_{HS}+ 60±1 % of Co^{III}_{LS} on the other hand. Contrasting the composition of the ground and excited-states, we deduce that 30±1 % of Co^{III}_{LS} are converted

into Co^{II}_{HS} while 28±1 % of the initial Fe^{II}_{LS} ions in the ground state are oxidized toward Fe^{III}_{LS} during laser irradiation. In other terms, and assuming an homogeneity in the sample, about one pair per {Tl ⊂ [Fe(2-TPhTp)$_4$Co(Tp)$_4$]} cage in the electropolymerized thin-film undergo a photo-induced conversion from Fe^{III}_{LS}-CN-Co^{III}_{LS} pairs to Fe^{II}_{LS}-CN-Co^{II}_{HS} ones. It is worth mentioning that the total irradiation time was 2h45, although further changes were observed on the spectra after 30 minutes of irradiation. The photo conversion appeared thus twice more effective in the starting material -for which two pairs are involved in the photo-conversion process- than in the electropolymerized thin-film. These outcomes are tentatively explained by (i) a sensitivity of the electropolymerized material toward oxidation, and/or (ii) a diversification of the environment of Fe and Co ions following the electropolymerization process, as assumed above, with some of the pairs inactive for the photoconversion.

Finally, the temperature-induced relaxation of the low temperature metastable excited state was tracked by warming up the electropolymerized films to 300 K. Figure 4 shows the x-ray absorption spectra obtained for Fe and Co at 300 K after irradiation at low temperature which demonstrate that the light-induced charge transfer in the film is fully reversible with temperature as the initial state was completely recovered after warming up the sample. While ramping up the temperature of the film, XAS at Fe and Co L_3 edges were collected at different temperatures between 2 and 180 K. At each temperature step, the L_3 edges of both ions were fitted with a linear combination of the above mentionned reference compounds of the metal ions (Figure S26). We observe a gradual decrease of the Fe^{III}_{LS} and Co^{II}_{HS} until the complete relaxation to the initial stable paramagnetic state. Hereby, the relaxation temperature was estimated at 62±5 K which is in very good agreement with the relaxation temperature of (**1**) obtained by measuring the variation of $\chi_M T$ as a function of temperature (Figure S16). Altogether, the XAS and XMCD investigations demonstrate an encouraging improvement in the deposition of the molecular building-block (**1**) on surface as thin-film without the loss of

its coveted photo-induced magnetic properties. These studies also open an interesting scope of investigations on further development of these new kind of multifunctional material which remains to date scarcely reported.

CONCLUSION

The deposition of a polymetallic molecular switch, a PBA{Fe_4Co_4} molecular unit, on a metallic surface as thin-film was successfully unlocked using an electrochemical approach as alternative to the ultra-high vacuum deposition process. Following a multistep synthetic route, the polymetallic {Fe_4Co_4} core was functionalized with thiophene substituents for harnessing their electrooxidative properties and processability, resulting thus in the {Tl $\subset$ [Fe^{II}(2-TPhTp)$(CN)_3$]$_4$[Co^{III}(Tp)]$_3$[Co^{II}(Tp)]} **(1)** versatile molecular complex. The electrochemical response of the electrogenerated material from (**1**) was typical of that of adsorbed species as inferred from the Randles-Sevcik equation. Surface characterization techniques revealed that the structural integrity of the molecular materials was maintained after electropolymerization on surfaces, without evidences of degradation. This latter aspect was unambigously demonstrated by XPS analyses which revealed a clear set of signals attributed to the expected redox state of the metal elements of the cage. Elemental composition of the thin-film probed by XPS was in good agreement with the stoichiometry of the cage's constitutive elements, corroborating the metals redox states and that its structure was preserved after electropolymerization. Under the experimental conditions defined in cyclic voltammetry, an homogenous growth of the electropolymerized film is achieved with a thickness of *ca*. 22 nm as unraveled by AFM measurements. Finally, XAS and XMCD results jointly indicate a preservation of the photoswitching property in the surface-electrodeposited material. Overall, the proof of concept detailed herein is to the best of our knowledge the first example of electropolymerized thin-film based on a polymetallic molecular switch. The solution processing route applied here led to a multifunctional thin-films combining the redox and

photomagnetic switchable properties of the molecular unit. It enlarges the scope of switchable molecular materials considered for molecule-based devices, the interest of which spans diverse research fields as optoelectronics devices, sensors or even spintronics -provided in the latter example an optimization of the relaxation temperature. To go further in this approach, we dedicated efforts in parallel to optimize the deposition of the octametallic cages as thin-films with a controlled thickness, which will be subject of an ensuing report.

Supporting Information
Supporting Information is available from the Wiley Online Library or from the author.

Acknowledgements
The authors are very grateful to Dalila Seghouane of the Mass Spectrometry department at Sorbonne Université for the HRMS analyses and Dr Jürgen Von Bardeleben from INSP for his help for EPR measurements. We also warmly thank Mr Kassymkhan Baiseitov for his participation in Synchrotron measurements. The supports of LABEX-MiChem (10-LABX-0068) and the MolSpin COST Action are gratefully acknowledged. N.D. and J.D. thank the Swiss National Science Foundation for funding (grant no. 200020_182599).

References

[1] M. A. Halcrow, *Spin-Crossover Materials: Properties and Applications*, John Wiley & Sons, **2013**.
[2] G. Chastanet, M. Lorenc, R. Bertoni, C. Desplanches, *Comptes Rendus Chimie* **2018**, *21*, 1075–1094.
[3] K. Yao, C. Dong, K. Cao, Y. Zhang, S. Yang, *Advanced Functional Materials* **2024**, *34*, 2313938.
[4] M. G. Reeves, E. Tailleur, P. A. Wood, M. Marchivie, G. Chastanet, P. Guionneau, S. Parsons, *Chem. Sci.* **2021**, *12*, 1007–1015.
[5] R. Sánchez-de-Armas, N. Montenegro-Pohlhammer, A. Develioglu, E. Burzurí, C. J. Calzado, *Nanoscale* **2021**, *13*, 18702–18713.
[6] N. A. A. M. Amin, S. M. Said, M. F. M. Salleh, A. M. Afifi, N. M. J. N. Ibrahim, M. M. I. M. Hasnan, M. Tahir, N. Z. I. Hashim, *Inorganica Chimica Acta* **2023**, *544*, 121168.
[7] G. Molnár, S. Rat, L. Salmon, W. Nicolazzi, A. Bousseksou, *Advanced Materials* **2018**, *30*, 1703862.
[8] L. Kipgen, M. Bernien, F. Tuczek, W. Kuch, *Advanced Materials* **2021**, *33*, 2008141.
[9] M. Gruber, R. Berndt, *Magnetochemistry* **2020**, *6*, 35.
[10] C. Lefter, V. Davesne, L. Salmon, G. Molnár, P. Demont, A. Rotaru, A. Bousseksou, *Magnetochemistry* **2016**, *2*, 18.
[11] S. Zerdane, M. Hervé, S. Mazerat, L. Catala, R. Alonso-Mori, J. M. Glownia, S. Song, M. Levantino, T. Mallah, M. Cammarata, E. Collet, *Faraday Discuss.* **2022**, *237*, 224–236.
[12] M. Cammarata, S. Zerdane, L. Balducci, G. Azzolina, S. Mazerat, C. Exertier, M. Trabuco, M. Levantino, R. Alonso-Mori, J. M. Glownia, S. Song, L. Catala, T. Mallah, S. F. Matar, E. Collet, *Nat. Chem.* **2021**, *13*, 10–14.
[13] M. Pénicaud, E. Martinez, G. Serrano, B. Cortigiani, L. Squillantini, J. H. González-Estefan, E. Velez-Fort, M. Duttine, M. Gonidec, P. Rosa, M. Mannini, L. Poggini, *J. Mater. Chem. C* **2023**, *11*, 11518–11528.
[14] L. Poggini, M. Milek, G. Londi, A. Naim, G. Poneti, L. Squillantini, A. Magnani, F. Totti, P. Rosa, M. M. Khusniyarov, M. Mannini, *Mater. Horiz.* **2018**, *5*, 506–513.
[15] T. Mallah, M. Cavallini, *Comptes Rendus Chimie* **2018**, *21*, 1270–1286.
[16] B. Warner, J. C. Oberg, T. G. Gill, F. El Hallak, C. F. Hirjibehedin, M. Serri, S. Heutz, M.-A. Arrio, P. Sainctavit, M. Mannini, G. Poneti, R. Sessoli, P. Rosa, *J. Phys. Chem. Lett.* **2013**, *4*, 1546–1552.
[17] E. Coronado, *Nat Rev Mater* **2020**, *5*, 87–104.
[18] V. Shalabaeva, K. Ridier, S. Rat, M. D. Manrique-Juarez, L. Salmon, I. Séguy, A. Rotaru, G. Molnár, A. Bousseksou, *Appl. Phys. Lett.* **2018**, *112*, 013301.

[19] G. Molnár, S. Rat, L. Salmon, W. Nicolazzi, A. Bousseksou, *Advanced Materials* **2018**, *30*, 1703862.
[20] Y. Zhang, R. Torres-Cavanillas, X. Yan, Y. Zeng, M. Jiang, M. Clemente-León, E. Coronado, S. Shi, *Chem. Soc. Rev.* **2024**, *53*, 8764–8789.
[21] O. Sato, T. Iyoda, A. Fujishima, K. Hashimoto, *Science* **1996**, *272*, 704–705.
[22] Y.-S. Meng, O. Sato, T. Liu, *Angewandte Chemie International Edition* **2018**, *57*, 12216–12226.
[23] D. Aguilà, Y. Prado, E. S. Koumousi, C. Mathonière, R. Clérac, *Chemical Society Reviews* **2016**, *45*, 203–224.
[24] T. Mahfoud, G. Molnár, S. Bonhommeau, S. Cobo, L. Salmon, P. Demont, H. Tokoro, S.-I. Ohkoshi, K. Boukheddaden, A. Bousseksou, *Journal of the American Chemical Society* **2009**, *131*, 15049–15054.
[25] Y.-B. Huang, J.-Q. Li, W.-H. Xu, W. Zheng, X. Zhang, K.-G. Gao, T. Ji, T. Ikeda, T. Nakanishi, S. Kanegawa, S.-Q. Wu, S.-Q. Su, O. Sato, *J. Am. Chem. Soc.* **2024**, *146*, 201–209.
[26] O. Sato, T. Kawakami, M. Kimura, S. Hishiya, S. Kubo, Y. Einaga, *J. Am. Chem. Soc.* **2004**, *126*, 13176–13177.
[27] M. Urdampilleta, C. Ayela, P.-H. Ducrot, D. Rosario-Amorin, A. Mondal, M. Rouzières, P. Dechambenoit, C. Mathonière, F. Mathieu, I. Dufour, R. Clérac, *Scientific Reports* **2018**, *8*, DOI 10.1038/s41598-018-26076-2.
[28] K. S. Kumar, M. Studniarek, B. Heinrich, J. Arabski, G. Schmerber, M. Bowen, S. Boukari, E. Beaurepaire, J. Dreiser, M. Ruben, *Advanced Materials* **2018**, *30*, 1705416.
[29] G. Gabarró-Riera, G. Aromí, E. C. Sañudo, *Coordination Chemistry Reviews* **2023**, *475*, 214858.
[30] T. Knaak, C. González, Y. J. Dappe, G. D. Harzmann, T. Brandl, M. Mayor, R. Berndt, M. Gruber, *J. Phys. Chem. C* **2019**, *123*, 4178–4185.
[31] T. G. Gopakumar, M. Bernien, H. Naggert, F. Matino, C. F. Hermanns, A. Bannwarth, S. Mühlenberend, A. Krüger, D. Krüger, F. Nickel, W. Walter, R. Berndt, W. Kuch, F. Tuczek, *Chemistry – A European Journal* **2013**, *19*, 15702–15709.
[32] S. Shi, G. Schmerber, J. Arabski, J.-B. Beaufrand, D. J. Kim, S. Boukari, M. Bowen, N. T. Kemp, N. Viart, G. Rogez, E. Beaurepaire, H. Aubriet, J. Petersen, C. Becker, D. Ruch, *Appl. Phys. Lett.* **2009**, *95*, 043303.
[33] N. Bridonneau, J. Long, J.-L. Cantin, J. von Bardeleben, D. R. Talham, V. Marvaud, *RSC Adv.* **2015**, *5*, 16696–16701.
[34] N. Daffé, F. Choueikani, S. Neveu, M.-A. Arrio, A. Juhin, P. Ohresser, V. Dupuis, P. Sainctavit, *Journal of Magnetism and Magnetic Materials* **2018**, *460*, 243–252.
[35] J. Glatz, J.-R. Jiménez, L. Godeffroy, H. J. von Bardeleben, L. Fillaud, E. Maisonhaute, Y. Li, L.-M. Chamoreau, R. Lescouëzec, *J. Am. Chem. Soc.* **2022**, *144*, 10888–10901.
[36] J.-R. Jiménez, M. Tricoire, D. Garnier, L.-M. Chamoreau, J. von Bardeleben, Y. Journaux, Y. Li, R. Lescouëzec, *Dalton Trans.* **2017**, *46*, 15549–15557.
[37] J.-D. Cafun, G. Champion, M.-A. Arrio, C. C. dit Moulin, A. Bleuzen, *Journal of the American Chemical Society* **2010**, *132*, 11552–11559.
[38] D. L. Reger, J. R. Gardinier, W. R. Gemmill, M. D. Smith, A. M. Shahin, G. J. Long, L. Rebbouh, F. Grandjean, *Journal of the American Chemical Society* **2005**, *127*, 2303–2316.
[39] D. L. Reger, J. R. Gardinier, S. BakbakCurrent address: School of Ch, R. F. Semeniuc, U. H. F. Bunz, M. D. Smith, *New Journal of Chemistry* **2005**, *29*, 1035.
[40] C. Pettinari, R. Pettinari, F. Marchetti, in *Advances in Organometallic Chemistry* (Ed.: P.J. Pérez), Academic Press, **2016**, pp. 175–260.

[41] A. Benchohra, C. Méthivier, J. Landoulsi, D. Kreher, R. Lescouëzec, *Chem. Commun.* **2020**, *56*, 6587–6589.
[42] K. Mitsumoto, H. Nishikawa, H. Oshio, *Polyhedron* **2011**, *30*, 3245–3248.
[43] Amina Benchohra, Magnetic Molecular Switches: From Their Synthesis to Their Integration into Hybrid (Nano)Materials, Ph.D. Thesis, Sorbonne Université, **2019**.
[44] Y. Qin, C. Cui, F. Jäkle, *Macromolecules* **2008**, *41*, 2972–2974.
[45] H. Vitze, M. Bolte, H.-W. Lerner, M. Wagner, *European Journal of Inorganic Chemistry* **2016**, *2016*, 2443–2454.
[46] D. Garnier, J.-R. Jiménez, Y. Li, J. von Bardeleben, Y. Journaux, T. Augenstein, E. M. B. Moos, M. T. Gamer, F. Breher, R. Lescouëzec, *Chem. Sci.* **2016**, *7*, 4825–4831.
[47] T. Shiga, N. Mihara, M. Nihei, *Coordination Chemistry Reviews* **2022**, *472*, 214763.
[48] D. Garnier, A. Mondal, Y. Li, P. Herson, L.-M. Chamoreau, L. Toupet, M. Buron Le Cointe, E. M. B. Moos, F. Breher, R. Lescouëzec, *Comptes Rendus Chimie* **2019**, *22*, 516–524.
[49] J. Jiménez, J. Glatz, A. Benchohra, G. Gontard, L. Chamoreau, J. Meunier, A. Bousseksou, R. Lescouëzec, *Angew. Chem. Int. Ed.* **2020**, *59*, 8089–8093.
[50] J. Roncali, *Chem. Rev.* **1992**, *92*, 711–738.
[51] F. A. Schultz, *J Solid State Electrochem* **2011**, *15*, 1833–1843.
[52] L. Groenendaal, G. Zotti, P.-H. Aubert, S. m. Waybright, J. r. Reynolds, *Advanced Materials* **2003**, *15*, 855–879.
[53] D. Briggs, *Surface and Interface Analysis* **1981**, *3*, v–v.
[54] N. Daffé, J.-R. Jiménez, M. Studniarek, A. Benchohra, M.-A. Arrio, R. Lescouëzec, J. Dreiser, *J. Phys. Chem. Lett.* **2019**, *10*, 1799–1804.